01 Nov 1988

A Neutron Diffraction and Mössbauer Spectral Study of the Structure and Magnetic Properties of the $Y_2Fe_{14-x}Si_xB$ Solid Solutions

Gaya Kanishka Marasinghe

Oran Allan Pringle
Missouri University of Science and Technology, pringle@mst.edu

Gary J. Long
Missouri University of Science and Technology, glong@mst.edu

William B. Yelon
Missouri University of Science and Technology

et. al. For a complete list of authors, see https://scholarsmine.mst.edu/phys_facwork/182

Recommended Citation

G. K. Marasinghe et al., "A Neutron Diffraction and Mössbauer Spectral Study of the Structure and Magnetic Properties of the $Y_2Fe_{14-x}Si_xB$ Solid Solutions," *Journal of Applied Physics*, vol. 76, no. 5, pp. 2960-2968, American Institute of Physics (AIP) Publishing, Nov 1988.
The definitive version is available at https://doi.org/10.1063/1.357536

A neutron diffraction and Mössbauer spectral study of the structure and magnetic properties of the $Y_2Fe_{14-x}Si_xB$ solid solutions

G. K. Marasinghe,[a] O. A. Pringle,[a] and Gary J. Long[b]
University of Missouri-Rolla, Rolla, Missouri 65401

W. B. Yelon
University of Missouri Research Reactor, Columbia, Missouri 65211

F. Grandjean
Institut de Physique, Université de Liège, B-4000 Sart Tilman, Belgium

(Received 13 December 1993; accepted for publication 26 May 1994)

A neutron diffraction and Mössbauer spectral study of $Y_2Fe_{14-x}Si_xB$ shows that silicon preferentially occupies the $4c$, and to a lesser extent, the $8j_1$ sites in $Y_2Fe_{14-x}Si_xB$. The trend in the site occupancy is the same as in $Nd_2Fe_{14-x}Si_xB$. The Curie temperature of $Y_2Fe_{14-x}Si_xB$ increases with increasing silicon content. Neutron diffraction data show that the increase in Curie temperature is accompanied by a contraction of the unit cell. Wigner–Seitz cell calculations, using the $Y_2Fe_{14-x}Si_xB$ lattice and positional parameters obtained by neutron diffraction, show that the silicon site occupancy is correlated with the rare earth contact area of that site. The Mössbauer spectra of $Y_2Fe_{14-x}Si_xB$ have been fit with a model which takes into account the distribution of near-neighbor environments of an iron atom due to the presence of silicon. The weighted average of H_{max}, the average hyperfine field of the iron sites with no silicon near neighbors, decreases by 42 and 45 kOe per silicon substitution per formula unit at 85 and 295 K, respectively. The weighted average of ΔH, the average reduction in the hyperfine field caused by the addition of one silicon near neighbor to the near neighbor environment, is about 13.5 and 18 kOe at 85 and 295 K, respectively, and does not show an appreciable dependence on the silicon content. The isomer shifts obtained from these fits suggest an increase in covalency of bonding on silicon substitution, an increase which is consistent with the preference of silicon to bond with yttrium.

I. INTRODUCTION

The substitution of small amounts of silicon for iron increases the Curie temperature of $R_2F_{14}B$ compounds by about 20 K per silicon atom substituted into the $R_2Fe_{14}B$ formula unit.[1] The most frequently invoked explanation for the increased Curie temperature has been that silicon reduces the extent of negative magnetic exchange interactions by preferentially replacing iron atoms on the sites in the $R_2Fe_{14}B$ structure which share the shorter iron–iron bond distances, specifically the $8j_1$ and $16k_2$ sites. However, more recent studies[2–5] of $Nd_2Fe_{14-x}Si_xB$ and $Y_2Fe_{14-x}Si_xB$ have shown that silicon preferentially occupies the $4c$ site, and to a lesser extent the $8j_1$ site, in the $R_2Fe_{14}B$ structure, and does not occupy the $16k_2$ site. The only apparent pattern to the occupancy is the preference of the silicon for coordination by the rare earth.[3,5]

A similar but even more dramatic increase in the Curie temperature occurs in the R_2Fe_{17} compounds.[6] The Curie temperature of $Nd_2Fe_{16}Si$ is about 70° higher than that of Nd_2Fe_{17}, and the magnetization direction changes[7] from basal in Nd_2Fe_{17} to axial in $Nd_2Fe_{17-x}Si_x$. Conventional arguments would place silicon on the $6c$ site in Nd_2Fe_{17}, the site which has a very short iron-$6c$ to near-neighbor iron-$6c$ bond. Instead, silicon preferentially occupies the $18h$ site[7] in $Nd_2Fe_{17-x}Si_x$, the site with the greatest number of neodymium near neighbors.

A better understanding of the mechanism by which silicon substitution increases the Curie temperature of $R_2Fe_{14}B$ may permit the formulation of better magnetic materials with improved Curie temperatures. Hence, we have undertaken a neutron diffraction study of $Y_2Fe_{14-x}Si_xB$ samples, with x values of 0.28, 0.67, and 1.87, on the powder diffractometer at the University of Missouri Research Reactor. Herein we report the results of this neutron diffraction study as well as Mössbauer spectral studies. In addition we report a Mössbauer effect study of samples with nominal x values of 1.0, 1.5, and 2.0. The results are used to relate the preferential silicon site occupation to the magnetic structure of $Y_2Fe_{14-x}Si_xB$.

II. EXPERIMENT

$Y_2Fe_{14-x}Si_xB$ samples, with nominal x values of 0.25, 0.75, and 1.75, were prepared as described earlier.[3] Small pieces of the annealed ingots were placed in a vibrating sample magnetometer and the magnetization was measured as a function of temperature between 295 and 700 K. The Curie temperatures were determined from the magnetic data and agreed well with those obtained earlier[1] for samples of the same nominal composition. The magnetization curves showed that the samples did not contain appreciable amounts of any secondary magnetic phases having Curie temperatures in the range of 295–700 K. Figure 1 shows the dependence of the Curie temperature on the silicon content in $Y_2Fe_{14-x}Si_xB$.

[a]Department of Physics.
[b]Department of Chemistry.

 0021-8979/94/76(5)/2960/9/$6.00

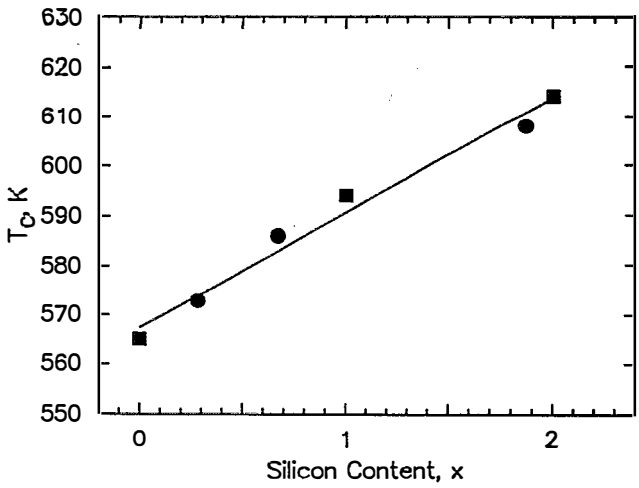

FIG. 1. The dependence of the Curie temperature on the silicon content in $Y_2Fe_{14-x}Si_xB$. The squares represent data taken from Ref. 1. The silicon contents used in this figure are those obtained from the neutron diffraction data refinements described in Sec. III of this article.

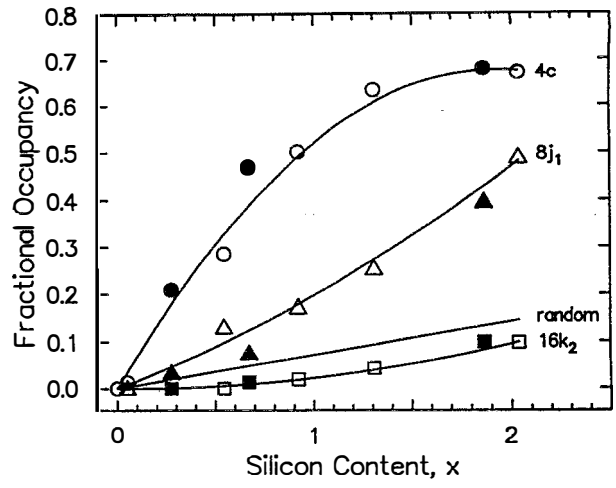

FIG. 2. Silicon occupancies for the $4c$, $16k_2$, and $8j_1$ sites for $Y_2Fe_{14-x}Si_xB$ (solid symbols) and $Nd_2Fe_{14-x}Si_xB$ (open symbols, from Ref. 3). The occupancies are plotted as N_{Si}/N, where N_{Si} is the number of silicon atoms occupying a site and N is the site crystallographic degeneracy. The line labeled "random" corresponds to silicon occupying all six transition metal sites with equal probability.

Each ingot was crushed under toluene and sieved to 400 mesh. The powdered samples were placed in thin-walled vanadium containers and powder neutron diffraction patterns were collected at the University of Missouri Research Reactor at temperatures of 295 and 8 K. The neutron wavelength was 1.289 Å. Each diffraction pattern was obtained in about 24 h. The data were rebinned into 0.1° steps and analyzed by using a modified Rietveld code which included a Voigt function to describe a mixed Gaussian–Lorentzian shape for the diffraction peaks. The neutron diffraction patterns at 295 and 8 K contained magnetic as well as nuclear scattering, both of which were refined simultaneously.

Mössbauer absorbers, with a typical thickness of 30 mg/cm^2, were made from the above materials as well as from samples prepared at Carnegie Mellon University and described elsewhere.[1,8] Mössbauer spectra of the $Y_2Fe_{14-x}Si_xB$ samples were obtained at 295 and 85 K on a Harwell spectrometer, which used a room temperature rhodium matrix cobalt-57 source and was calibrated at room temperature with α-iron foil. The spectra were fit by assuming a binomial distribution of iron and silicon in the near-neighbor environment at each iron site, a distribution which is based on the silicon occupancies determined by neutron diffraction.

III. NEUTRON DIFFRACTION RESULTS

The $Y_2Fe_{14-x}Si_xB$ samples crystallized in the $Nd_2Fe_{14}B$ structure.[9] The crystallographic site occupancies have been previously reported.[5] The $16k_1$, $8j_2$, and $4e$ sites are fully populated by iron, whereas silicon is present only on the $16k_2$, $8j_1$, and $4c$ transition metal sites. The refined atomic positions are essentially the same as those found in $Nd_2Fe_{14}B$. When the total silicon content was allowed to vary, the nominal x values of 0.25, 0.75, and 1.75 refined to 0.28±0.03, 0.67±0.05, and 1.87±0.07, respectively. The refined silicon occupancies are given in Table I and plotted as a function of silicon content in Fig. 2. At low silicon concentrations, silicon clearly prefers the $4c$ site, and silicon occupies this site almost exclusively in $Y_2Fe_{13.72}Si_{0.28}B$ and $Y_2Fe_{13.33}Si_{0.67}B$. Only in $Y_2Fe_{12.13}Si_{1.87}B$ is there any significant occupation of the $8j_1$ site, and in $Y_2Fe_{12.13}Si_{1.87}B$ the occupation of the $16k_2$ site is less than the expected value if silicon were to occupy all sites randomly. There was no indication in the refinements that any silicon resides on the $4e$, $8j_2$, or $16k_1$ sites.

The $Y_2Fe_{14-x}Si_xB$ samples are all magnetically ordered at 295 and 8 K. The same refinement techniques used[3] for $Nd_2Fe_{14-x}Si_xB$ were also used in the refinement of the

TABLE I. Silicon site occupancies, N_{Si}, and percent silicon site occupancies per unit cell in $Y_2Fe_{14-x}Si_xB$.

	$Y_2Fe_{13.72}Si_{0.28}B$		$Y_2Fe_{13.33}Si_{0.67}B$		$Y_2Fe_{12.13}Si_{1.87}B$	
Site	N_{Si}	%Si	N_{Si}	%Si	N_{Si}	%Si
$16k_2$	0.0	0.0	0.21±0.14	1.3±0.9	1.58±0.20	9.9±1.3
$8j_1$	0.27±0.11	3.3±1.4	0.60±0.10	7.5±1.2	3.17±0.14	39.6±1.7
$4c$	0.84±0.08	20.9±2.1	1.88±0.07	47.0±1.7	2.72±0.10	68.0±2.6
Total	0.28±0.03	2.0±0.2	0.67±0.05	4.8±0.3	1.87±0.07	13.3±0.5

TABLE II. Results of neutron diffraction refinements for $Y_2Fe_{14-x}Si_xB$ at 295 K.[a,b]

Parameter	$Y_2Fe_{13.72}Si_{0.28}B$	$Y_2Fe_{13.33}Si_{0.67}B$	$Y_2Fe_{12.13}Si_{1.87}B$
	Atomic Coordinates		
Y 4*f* *x*	0.2653(6)	0.2688(6)	0.2678(8)
Y 4*g* *x*	0.1449(7)	0.1427(6)	0.1496(9)
Fe 16k_1 *x*	0.2222(4)	0.2231(4)	0.2213(6)
Fe 16k_1 *y*	0.5682(4)	0.5676(3)	0.5728(5)
Fe 16k_1 *z*	0.1276(3)	0.1284(2)	0.1293(4)
Fe 16k_2 *x*	0.0383(4)	0.0373(3)	0.0383(6)
Fe 16k_2 *y*	0.3598(4)	0.3594(3)	0.3604(6)
Fe 16k_2 *z*	0.1740(3)	0.1738(2)	0.1732(4)
Fe 8j_1 *x*	0.0968(5)	0.0973(4)	0.1019(7)
Fe 8j_1 *z*	0.2001(3)	0.1992(3)	0.1995(5)
Fe 8j_2 *x*	0.3172(4)	0.3165(3)	0.3155(5)
Fe 8j_2 *z*	0.2455(5)	0.2458(4)	0.2476(5)
Fe 4*e* *z*	0.1175(7)	0.1163(5)	0.1156(9)
B 4*g* *x*	0.3698(12)	0.3713(11)	0.3651(5)
	Magnetic Moments, μ_B		
Fe 16k_1	2.0(1)	2.1(1)	1.4(2)
Fe 16k_2	1.9(1)	1.5(1)	0.7(1)
Fe 8j_1	1.0(1)	1.0(1)	1.8(3)
Fe 8j_2	2.7(2)	2.6(1)	2.8(1)
Fe 4*e*	2.0(1)	1.9(1)	2.1(1)
Fe 4*c*	1.5(1)	1.4(1)	1.6(1)
M/f.u.[c]	26.1	24.0	18.6
	Lattice Parameters and Unit Cell Volume		
a, Å	8.7469(8)	8.7291(7)	8.7061(11)
c, Å	12.0159(13)	11.9966(12)	11.9444(21)
c/*a*	1.3737(2)	1.3743(2)	1.3720(3)
V, Å^3	919.3(2)	914.1(2)	905.3(3)
	R-Factors and Residual		
R(%)	5.00	3.90	6.43
$R_{expected}$(%)	3.08	3.06	3.30
$R_{nuclear}$(%)	4.93	3.84	6.29
$R_{magnetic}$(%)	6.97	5.91	11.50
Residual	7.07	4.66	9.45

[a]Silicon atomic coordinates and thermal parameters are the same as the iron coordinates and thermal parameters for the same site. The silicon site occupancies used in these refinements are given in Table I.
[b]The numbers in parentheses in this and subsequent tables are the standard deviations in the final digits of the refined values.
[c]Magnetization per formula unit.

TABLE III. Results of neutron diffraction refinements for $Y_2Fe_{14-x}Si_xB$ at 8 K.[a]

Parameter	$Y_2Fe_{13.72}Si_{0.28}B$	$Y_2Fe_{13.33}Si_{0.67}B$	$Y_2Fe_{12.13}Si_{1.87}B$
	Atomic Coordinates		
Y 4*f* *x*	0.2639(8)	0.2666(6)	0.2695(10)
Y 4*g* *x*	0.1416(8)	0.1429(7)	0.1481(10)
Fe 16k_1 *x*	0.2232(5)	0.2240(4)	0.2236(6)
Fe 16k_1 *y*	0.5672(4)	0.5673(4)	0.5694(5)
Fe 16k_1 *z*	0.1280(3)	0.1285(3)	0.1274(4)
Fe 16k_2 *x*	0.0367(4)	0.0369(4)	0.0347(6)
Fe 16k_2 *y*	0.3604(4)	0.3605(4)	0.3615(6)
Fe 16k_2 *z*	0.1742(3)	0.1741(3)	0.1744(4)
Fe 8j_1 *x*	0.0966(5)	0.0970(4)	0.1011(8)
Fe 8j_1 *z*	0.1995(4)	0.1994(3)	0.1995(6)
Fe 8j_2 *x*	0.3168(4)	0.3171(4)	0.3143(5)
Fe 8j_2 *z*	0.2462(5)	0.2466(4)	0.2476(6)
Fe 4*e* *z*	0.1147(7)	0.1144(6)	0.1153(9)
B 4*g* *x*	0.3688(12)	0.3701(12)	0.3696(16)
	Magnetic Moments, μ_B		
Fe 16k_1	1.7(2)	2.1(1)	1.3(2)
Fe 16k_2	1.9(2)	1.3(1)	2.1(2)
Fe 8j_1	2.7(2)	2.7(1)	2.2(2)
Fe 8j_2	3.3(2)	3.3(1)	2.6(2)
Fe 4*e*	2.4(3)	2.4(1)	1.9(1)
Fe 4*c*	1.8(3)	1.9(1)	1.5(1)
M/f.u.[b]	30.2	28.5	22.8
	Lattice Parameters and Unit Cell Volume		
a, Å	8.7442(9)	8.7166(8)	8.6856(11)
c, Å	11.9920(15)	11.9713(14)	11.9205(20)
c/*a*	1.3714(2)	1.3734(2)	1.3724(3)
V, Å^3	916.9(3)	909.6(2)	899.3(3)
	R-Factors and Residual		
R(%)	4.01	4.10	7.27
$R_{expected}$(%)	2.74	2.69	3.29
$R_{nuclear}$(%)	3.95	3.99	7.23
$R_{magnetic}$(%)	5.34	6.59	8.78
Residual	8.56	7.29	12.61

[a]Silicon atomic coordinates and thermal parameters are the same as the iron coordinates and thermal parameters for the same site. The silicon site occupancies used in these refinements are given in Table I.
[b]Magnetization per formula unit.

$Y_2Fe_{14-x}Si_xB$ magnetic scattering. In magnetic refinements of $Y_2Fe_{14-x}Si_xB$, the iron magnetic moments were constrained to lie along the *c* axis, and the vector sum of the magnetic moments was constrained to equal the bulk moment calculated by interpolation of the magnetization data given in Ref. 1. The samples contain from 3% to 5% of α-iron. The regions in the diffraction pattern which included the α-iron reflections, amounting to about 10% of the 450 observed reflections, were excluded from the refinements. Tables II and III give the atomic coordinates, magnetic moments, lattice parameters, and *R* factors resulting from the refinements of neutron diffraction patterns at 295 and 8 K, respectively.

In the magnetic refinements shown in Table II, the $8j_1$ site magnetic moments were constrained so that the $8j_1$ to $8j_2$ magnetic moment ratio was the same as in $Nd_2Fe_{14}B$. Releasing this constraint gave only slightly better *R* factors and residuals, but resulted in unreasonably large magnetic moments on the $8j_2$ site. Because the magnetic scattering is weak, amounting to about 5% or less of the total scattering, the atomic positional and occupancy parameters are insensitive to the details of the magnetic structure, and it is appropriate to build constraints into the magnetic structure to ensure consistency with the known magnetic structures of $Y_2Fe_{14}B$, $Nd_2Fe_{14}B$, and related compounds. Except for $Y_2Fe_{12.13}Si_{1.87}B$, where the magnetic scattering is the weakest, the magnetic *R* factors are quite reasonable, and the individual iron magnetic moments follow trends similar to those found in $Y_2Fe_{14}B$ and $Nd_2Fe_{14}B$ at 295 and 77 K.[10]

The unit cell dimensions and volume, as a function of composition, are shown in Fig. 3. The 295 K lattice and atomic positional parameters were used to calculate[11] the compositional dependence of the Wigner–Seitz cell volumes in $Y_2Fe_{14-x}Si_xB$ and the results are shown in Fig. 4. In these calculations, the radius used for those sites containing both iron and silicon was the composition weighted average of 1.26 Å for iron and 1.32 Å for silicon, the values appropriate for a 12 near-neighbor metallic lattice. Radii of 1.78 and 0.98 Å were used for yttrium and boron, respectively. Figure 4 indicates that there are distinct differences in the composition

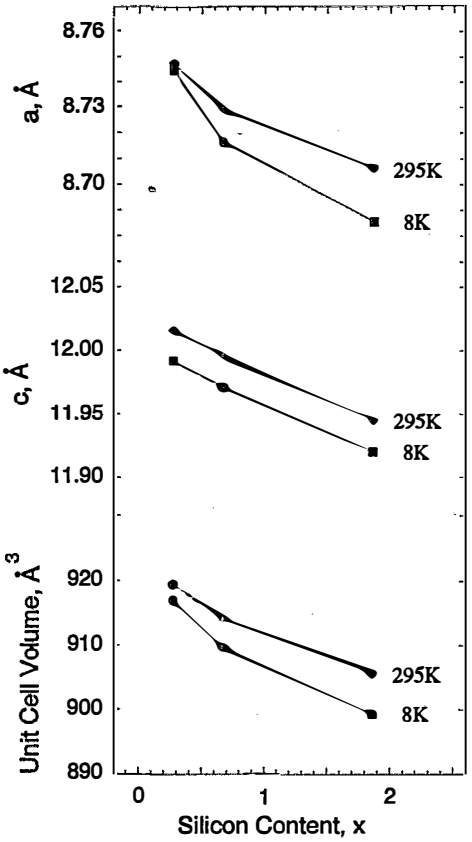

FIG. 3. The compositional dependence of the lattice parameters and unit cell volume for $Y_2Fe_{14-x}Si_xB$.

dependence of the Wigner–Seitz cell volume for the different iron sites. Although, as expected, the volumes of the $16k_1$, $16k_2$, and $8j_2$ sites decrease with increasing silicon content, the volumes of the $8j_1$, $4e$, and $4c$ sites increase slightly with increasing silicon content. The varied dependences of different site volumes on the silicon content indicates that the silicon substitution is accompanied by nonuniform structural changes in the unit cell.

IV. MÖSSBAUER SPECTRAL RESULTS

The Mössbauer spectra were initially fit with six broadened magnetic sextets, corresponding to the six crystallographically distinct iron sites in $Y_2Fe_{14-x}Si_xB$. The relative areas of the sextets were determined from the silicon occupation values obtained from neutron diffraction and given in Table I. In these initial fits, the area weighted average hyperfine field decreases by 40 and 47 kOe per silicon substituted for iron at 295 and 85 K, respectively. As expected on the basis of the relative electronegativities of silicon and iron, the area weighted average isomer shift shows a small increase with increasing silicon content.

In the above fits, all iron atoms on a specific lattice site are assumed to have the same hyperfine parameters, independent of their near-neighbor environment. However, in the partially silicon-substituted compounds, the near-neighbor environment of any particular iron atom is influenced by the presence of silicon. The variation in the near-neighbor environment for a specific iron site produces a distribution of the hyperfine parameters for that site. By assuming that silicon is substituted randomly on the $4c$, $8j_1$, and $16k_2$ sites, with site occupancies as determined by neutron diffraction, the binomial distribution of silicon near neighbors for a specific iron site can be calculated.

The Mössbauer spectra have been fit with a model which takes into account the distribution of near-neighbor environments. In this fitting procedure,[3,12] the iron atoms belonging to a given type of crystallographic site are represented by a group of magnetic sextets. Each sextet in this group represents the iron atoms having a different number of silicon near neighbors, and the relative area of this sextet is determined by the probability, as determined from the binomial distribution, of an iron atom having the corresponding number of silicon near neighbors. Both the maximum hyperfine field, H_{max}, for the iron atoms on a specific site which has zero silicon near neighbors, and an incremental field, ΔH, the change in the hyperfine field when one silicon replaces an iron atom in the near-neighbor environment of the site, have been determined. In this approach, for a specific silicon concentration, x, the internal hyperfine field, $H_{int}(x,n)$, at an iron atom with n silicon near neighbors, is given by $H_{int}(x,n)=H_{max}(x)-n\Delta H(x)$.

The initial values for the isomer shifts were taken from the fits which used broadened lines to approximate the distribution of near-neighbor environments. The quadrupole interactions were calculated from the quadrupole shifts from the line-broadened fits, and the angles, θ, between the hyperfine field and the principal axis of the electric field gradient tensor at each iron site.[13] The binomial distribution fits of the Mössbauer spectra of $Y_2Fe_{14-x}Si_xB$, obtained at 85 K, are shown in Fig. 5. The 85 K fits included only the samples for which site occupancies were available from neutron diffraction. The site occupancies for the remaining samples included in the 295 K fits were obtained by interpolation to the nominal silicon occupancy. The hyperfine parameters derived from the binomial fits of the spectra obtained at 295 and 85 K are given in Tables IV and V, respectively. The

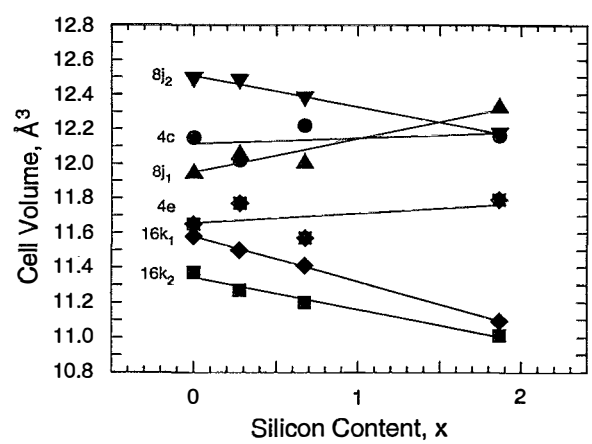

FIG. 4. The compositional dependence of the 295 K Wigner–Seitz cell volumes in $Y_2Fe_{14-x}Si_xB$.

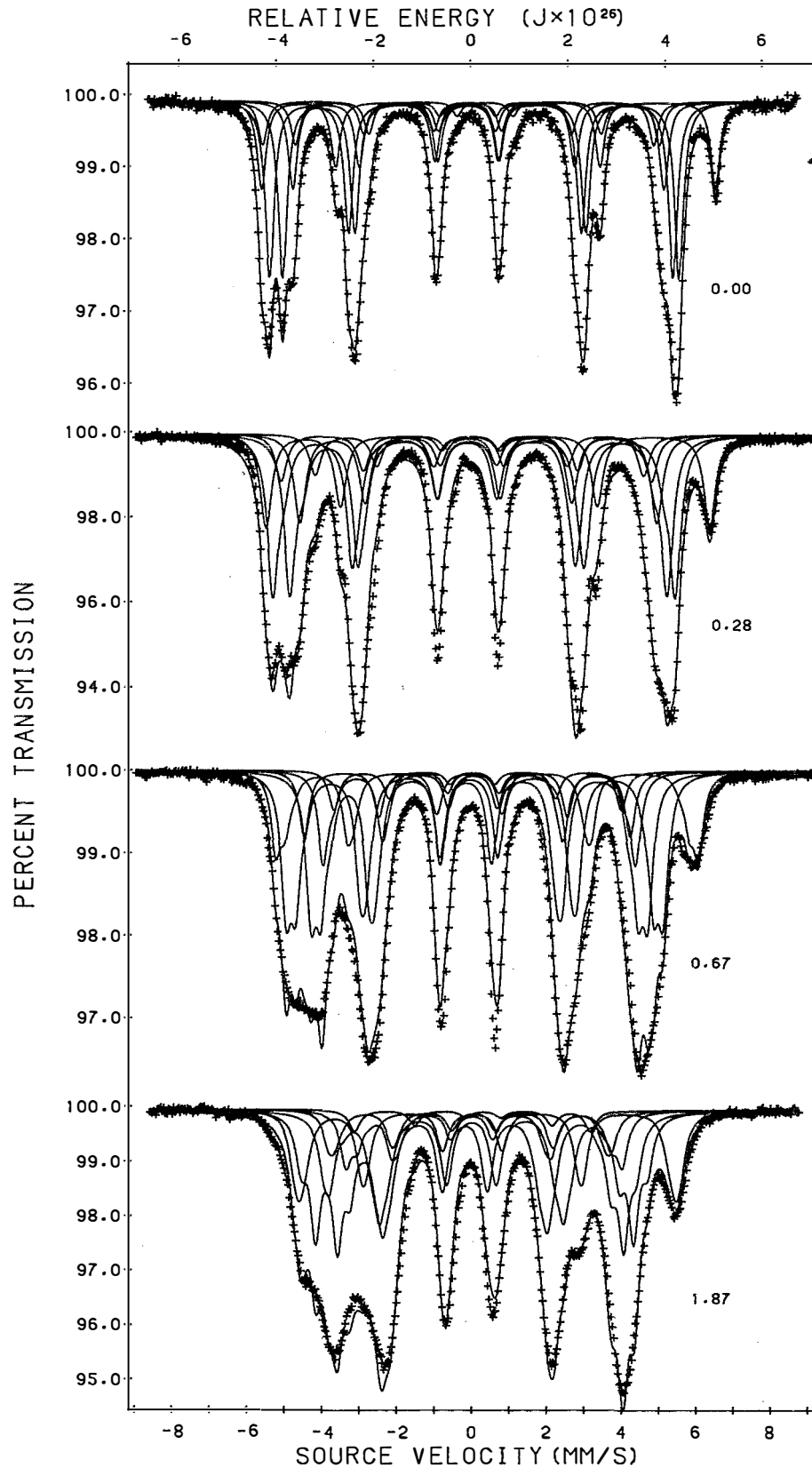

FIG. 5. The Mössbauer spectra of $Y_2Fe_{14-x}Si_xB$, obtained at 85 K and fit with a binomial distribution of silicon atoms in the near-neighbor environment of each iron site.

TABLE IV. Hyperfine parameters obtained from distribution fits of the Mössbauer spectra of $Y_2Fe_{14-x}Si_xB$ obtained at 295 K.

Parameter	x	Site $16k_1$	$16k_2$	$8j_1$	$8j_2$	$4e$	$4c$	W. Avg.
H_{max}, kOe	0.00	277	289	259	327	281	253	280
	0.28	265	285	246	320	263	234	267
	0.67	243	271	226	307	235	194	245
	1.00	237	268	218	301	225	183	230
	1.50	228	253	202	287	203	172	212
	1.87	221	248	196	280	196	166	202
	2.00	218	242	188	280	187	175	194
ΔH, kOe	0.28	13.0	12.0	...	...	...	...	12.5
	0.67	13.6	14.0	13.6	14.1	...	...	13.8
	1.00	12.2	16.3	13.5	10.1	...	...	13.3
	1.50	14.5	19.9	14.0	6.1	...	...	14.4
	1.87	13.7	20.2	15.0	5.9	...	...	14.6
	2.00	14.6	19.7	14.3	6.0	...	...	14.5
δ,[a] mm/s	0.00	−0.062	−0.117	−0.091	0.065	−0.083	−0.071	−0.056
	0.28	−0.067	−0.108	−0.087	0.063	−0.080	−0.027	−0.056
	0.67	−0.064	−0.096	−0.001	0.078	−0.090	0.001	−0.042
	1.00	−0.063	−0.093	0.017	0.065	−0.116	0.021	−0.040
	1.50	−0.044	−0.062	0.060	0.114	−0.150	0.100	−0.015
	1.87	−0.045	−0.031	0.080	0.116	−0.150	0.140	−0.005
	2.00	−0.028	−0.039	0.100	0.157	−0.157	0.190	0.007
θ, degrees	...	17.8	32.9	2.5	11.5	0	90	...
ΔE_Q, mm/s	0.00	0.273	0.264	0.260	0.543	−0.403	−0.542	...
	0.28	0.291	0.241	0.335	0.523	−0.127	−0.406	...
	0.67	0.358	0.218	0.296	0.516	−0.139	−0.646	...
	1.00	0.368	0.210	0.341	0.515	−0.116	−0.710	...
	1.50	0.348	0.174	0.343	0.473	−0.150	−0.800	...
	1.87	0.329	0.259	0.447	0.419	−0.177	−0.799	...
	2.00	0.292	0.154	0.382	0.435	−0.098	−1.081	...

[a]Relative to α-iron foil at 295 K.

TABLE V. Hyperfine parameters obtained from distribution fits of the Mössbauer spectra of $Y_2Fe_{14-x}Si_xB$ obtained at 85 K.

Parameter	x	Site $16k_1$	$16k_2$	$8j_1$	$8j_2$	$4e$	$4c$	W. Avg.
H_{max}, kOe	0.00	322	338	307	375	329	296	322
	0.28	313	333	294	368	307	268	313
	0.67	280	310	257	350	270	238	281
	1.87	258	287	229	321	235	194	240
ΔH, kOe	0.28	22.0	19.0					20.4
	0.67	16.0	16.3	18.0	15.3			16.4
	1.87	21.3	23.4	19.0	8.3			19.1
δ,[a] mm/s	0.00	0.061	0.000	0.044	0.206	0.040	0.027	0.062
	0.28	0.045	0.003	0.056	0.189	−0.077	0.118	0.050
	0.67	0.046	0.021	0.109	0.189	−0.029	0.100	0.062
	1.87	0.049	0.056	0.191	0.245	0.022	0.177	0.089
θ, degrees		17.8	32.9	2.5	11.5	0	90	
ΔE_Q, mm/s	0.00	0.297	0.348	0.328	0.591	−0.410	−0.328	
	0.28	0.356	0.268	0.263	0.542	−0.121	−0.388	
	0.67	0.418	0.280	0.356	0.515	−0.163	−0.286	
	1.87	0.491	0.246	0.335	0.439	−0.075	−0.589	

[a]Relative to α-iron foil at 295 K.

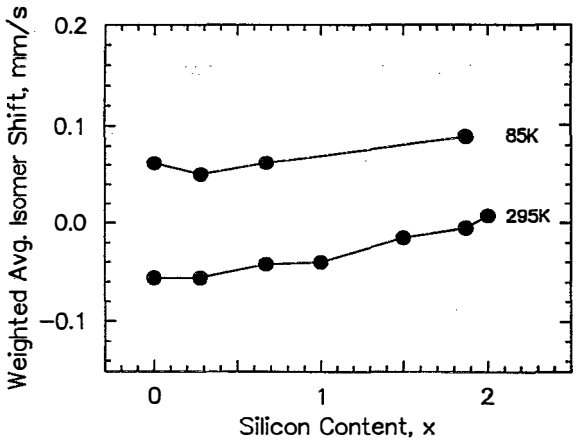

FIG. 6. The 295 and 85 K compositional dependence of the weighted average isomer shifts in $Y_2Fe_{14-x}Si_xB$.

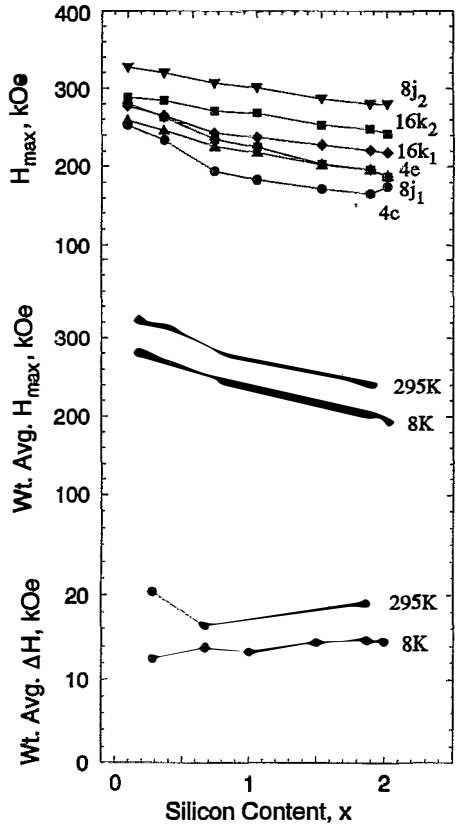

FIG. 7. The 295 K compositional dependence of H_{max}, and the 295 and 85 K compositional dependence of the site weighted average of H_{max} and ΔH in $Y_2Fe_{14-x}Si_xB$.

weighted average isomer shifts are shown in Fig. 6 as a function of silicon content.

The variation with silicon content of H_{max} for each site at 295 K and the site weighted average values of H_{max} and ΔH at 85 and 295 K are shown in Fig. 7. For all iron sites, H_{max} decreases uniformly with increasing silicon content. The site weighted average value of H_{max} decreases by 42 and 45 kOe per silicon substituted for iron at 295 and 85 K, respectively. The weighted average of ΔH is independent of the overall silicon concentration, and is in the range of 12–20 kOe. The Mössbauer results are in general very similar to those[3] of $Nd_2Fe_{14-x}Si_xB$.

V. DISCUSSION

The effects of silicon substitution on the Curie temperature, lattice parameters, magnetic moments, and Mössbauer hyperfine parameters of $Y_2Fe_{14-x}Si_xB$ are very similar to those found[3] for $Nd_2Fe_{14-x}Si_xB$. The magnetic moments and the hyperfine fields in the $Y_2Fe_{14-x}Si_xB$ compounds are slightly smaller than in $Nd_2Fe_{14-x}Si_xB$, but this difference is expected because the yttrium atoms have no magnetic moment. It is reasonable to conclude that the mechanism by which the addition of silicon increases the Curie temperature of $Y_2Fe_{14}B$ is the same as that in $Nd_2Fe_{14}B$, which has been previously discussed in some detail.[3]

The preferential occupancy of the 4*c* site by silicon is unusual for $R_2Fe_{14}B$. Preferential site occupancies by aluminum,[14] cobalt,[15] and maganese[16] $R_2Fe_{14-x}T_xB$ compounds are well understood on the basis of the relative atomic volumes of the various sites. The same volume argument, applied to $R_2Fe_{14-x}Si_xB$, would place silicon on the largest transition metal site, the $8j_2$ site, which has the largest Wigner–Seitz cell volume.[11] The 4*c* and $8j_1$ sites, for which silicon has the strongest preference, are the second and third largest sites. Therefore, the silicon site occupancy cannot be explained by site-filling volume considerations alone.

The silicon affinity for a given transition metal site is correlated with the number of rare earth near neighbors for that site. The rare earth coordination of a transition metal site can be expressed as the percentage surface area that is shared

TABLE VI. Percentage of the Wigner–Seitz cell surface area shared by iron and its rare earth near neighbors.

$Y_2Fe_{14}B$			$Nd_2Fe_{14}B$			Nd_2Fe_{17}		
Site	% RE contact area	% Si occupancy in $Y_2Fe_{12.13}Si_{1.87}B$	Site	% RE contact area	% Si occupancy in $Nd_2Fe_{11.96}Si_{2.04}B$	Site	% RE contact area	% Si occupancy in $Nd_2Fe_{12.91}Si_{4.09}$
$16k_1$	19.1	0	$16k_1$	19.3	0	6*c*	10.6	0
$16k_2$	18.6	9.9	$16k_2$	18.7	9.7	9*d*	13.1	15
$8j_1$	25.2	39	$8j_1$	26.6	49	18 *f*	21.2	20.8
$8j_2$	19.9	0	$8j_2$	19.8	0	18*h*	27.4	39.8
4*e*	16.9	0	4*e*	18.7	0	...	...	...
4*c*	30.5	68	4*c*	30	67	...	...	...

TABLE VII. Electronegativities of substitutional elements, T, and the dependence of the Mössbauer effect isomer shifts on the substitutional concentration in $R_2Fe_{14-x}T_xB$.

R	T	Electronegativity of T[a]	Electronegativity difference[b]	Isomer shift Change, mm/s[c]	Reference
Nd	Fe	1.64	...	...	...
Nd	Al	1.47	−0.17	−0.002	14
Nd	Co	1.7	0.06	−0.012	15
Nd	Mn	1.60	−0.04	−0.013	16
Nd	Si	1.74	0.1	0.036	3
Y	Si	1.74	0.1	0.035	...

[a]Allred–Rochow electronegativity.
[b]With respect to the electronegativity of Fe.
[c]Rate of change of Mössbauer effect isomer shift, per substituted atom per formula unit.

with its rare earth near neighbors. These percentages, obtained from Wigner–Seitz cell calculations for $Y_2Fe_{14}B$, $Nd_2Fe_{14}B$, and Nd_2Fe_{17}, are given in Table VI, along with the percentage silicon site occupancies[3,7] in $Y_2Fe_{12.13}Si_{1.87}B$, $Nd_2Fe_{11.96}Si_{2.04}B$, and $Nd_2Fe_{12.91}Si_{4.09}$. The correlation between the number of rare earth near-neighbors and silicon occupancy is high for all compounds. The silicon site occupancies are given for the samples with the largest silicon content, but the correlation is even more pronounced for $Y_2Fe_{14-x}Si_xB$ and $Nd_2Fe_{14-x}Si_xB$ with lower silicon content because the relative silicon affinity for the $4c$ site is greater at smaller silicon content.

The basis for the silicon affinity for a transition metal site with rare earth near neighbors can be explained in terms of the principles first proposed by Hume–Rothery,[17] who showed that all metals have a tendency to form normal valence bonds with the elements of the groups[18] IV_B, V_B, and VI_B. Furthermore, the more electropositive the metal and the more electronegative the B subgroup element, the greater the tendency to form valence bonds. Of the transition metal substitutions which have been investigated by neutron diffraction of Mössbauer spectroscopy, namely aluminum, cobalt, manganese, and silicon, only silicon belongs to the B subgroup of elements. Furthermore, the rare earth atoms are much more electropositive, having an Allred–Rochow electronegativity of approximately 1.1, than are the iron atoms, whose electronegativity is 1.90. Consequently, silicon can be expected to show a higher affinity for those transition metal sites which have higher levels of rare earth coordination. These sites are the $4c$ and $8j_1$ sites in the $R_2Fe_{14}B$ compounds and the $18h$ and $18f$ sites in the R_2Fe_{17} compounds. It is interesting that the isomer shift in $Nd_2Fe_{14-x}Si_xB$ and $Y_2Fe_{14-x}Si_xB$ increases with increasing silicon content even though the volume of the unit cell decreases.[3] A similar behavior is also found in $Nd_2Fe_{17-x}Si_x$. This increase is in agreement with the change expected on the basis of the higher electronegativity of silicon as compared to iron, see Table VII.

The above covalency argument does not lead to the conclusion that the rare earth–silicon bonds are purely covalent. Instead, it is reasonable to assume that the rare earth–silicon and iron–silicon bonds have a relatively higher degree of covalency than the equivalent rare earth–iron or iron–iron bonds. An analysis of the $Nd_2Fe_{14-x}Si_xB$ and $Y_2Fe_{14-x}Si_xB$ isomer shifts indicates that the covalent nature of bonding increases with increasing silicon content. The dependence of the Mössbauer effect isomer shift on the substituent concentration has previously been associated with the difference between the electronegativities of the substituent atom and iron.[3,7,16] The electronegativity difference is expected to influence the contribution made to the isomer shift by altering the s-electron density at the remaining iron nuclei. However, a comparison of the effects of different substituents on the Mössbauer isomer shifts of $Nd_2Fe_{14-x}T_xB$ and $Y_2Fe_{14-x}T_xB$, where T is Al, Co, Mn, and Si, as shown in Table VII, indicates that the mechanism by which silicon increases the isomer shift may be different from that of aluminum, cobalt, and manganese. As the covalent nature of bonding increases, the Mössbauer effective recoil mass, M_{eff}, of the iron-57 should increase, resulting in an increase in the isomer shift, in addition to the increase caused by the higher electronegativity of the silicon atoms. As shown in Table VIII, M_{eff}, which is calculated from the temperature dependence of the isomer shift,[19] increases with silicon content. Consequently, the isomer shift in the $R_2Fe_{14-x}T_xB$ compounds has a larger positive dependence on the silicon content than on aluminum, cobalt, or manganese content, as is shown in Table VII.

TABLE VIII. M_{eff} of the iron-57 nuclei as calculated from the temperature dependence of the weighted average isomer shifts in $Y_2Fe_{14-x}Si_xB$.

x	M_{eff}
0.0	74.0
0.28	82.4
0.67	84.0
1.87	92.7

ACKNOWLEDGMENTS

The authors acknowledge the support of the U.S. National Science Foundation through grant DMR-92-14271, and NATO for a Cooperative Scientific Research Grant (92-1160). G. J. Long thanks the Commission for Educational Exchange between the United States of America, Belgium, and Luxemburg for a Fulbright Research Fellowship during the 1993–94 academic year. The authors also thank Professor W. E. Wallace for providing the $Y_2Fe_{13}SiB$, $Y_2Fe_{12.5}Si_{1.5}B$, and $Y_2Fe_{12}Si_2B$ samples, from which Mössbauer effect results were obtained, and Dr. A. Basanginonga for his assistance in writing the binomial distribution fitting program.

[1] A. T. Pedziwiatr and W. E. Wallace, J. Less-Common Metals **126**, 41 (1986).
[2] S. Brennan, A. Bienenstock, and J. E. Keem, J. Appl. Phys. **65**, 697 (1988).
[3] G. K. Marasinghe, O. A. Pringle, G. J. Long, W. J. James, D. Xie, J. Li, W. B. Yelon, and F. Grandjean, J. Appl. Phys. **74**, 6798 (1993).
[4] Y. C. Yang, F. Xing, L. S. Kong, J. L. Yang, Y. F. Ding, B. S. Zhang, C. T. Ye, L. Jin, and H. M. Zhou, J. Phys. (Paris) Colloq. **49**, C8-597 (1988).
[5] G. K. Marasinghe, O. A. Pringle, G. J. Long, F. Grandjean, and W. B. Yelon, IEEE Trans. Magn. **29**, 2764 (1993).

[6] R. van Mens, J. Magn. Magn. Mater. **61**, 24 (1986).
[7] G. J. Long, G. K. Marasinghe, S. Mishra, O. A. Pringle, F. Grandjean, K. H. J. Buschow, D. P. Middleton, W. B. Yelon, F. Pourarian, and O. Isnard, Solid State Commun. **88**, 761 (1994).
[8] O. A. Pringle, G. J. Long, G. K. Marasinghe, W. J. James, A. T. Pedziwiatr, W. E. Wallace, and F. Grandjean, IEEE Trans. Magn. **MAG-25**, 3440 (1989).
[9] J. F. Herbst, J. J. Croat, F. E. Pinkerton, and W. B. Yelon, Phys. Rev. B **29**, 4176 (1984).
[10] J. F. Herbst, J. J. Croat, and W. B. Yelon, J. Appl. Phys. **57**, 4086 (1985).
[11] L. Gelato, J. Appl. Cryst. **14**, 141 (1981).
[12] D. E. Tharp, G. J. Long, O. A. Pringle, G. K. Marasinghe, W. J. James, and F. Grandjean, J. Appl. Phys. **64**, 5583 (1988).
[13] F. Grandjean, G. J. Long, D. E. Tharp, O. A. Pringle, and W. J. James, J. Phys. (Paris) Colloq. **49**, C8-581 (1988).
[14] Y. C. Yang, D. E. Tharp, G. J. Long, O. A. Pringle, and W. J. James, J. Appl. Phys. **61**, 4343 (1987).
[15] J. F. Herbst and W. B. Yelon, J. Appl. Phys. **60**, 4224 (1986).
[16] G. K. Marasinghe, O. A. Pringle, G. J. Long, W. J. James, W. B. Yelon, D. Xie, and F. Grandjean, J. Appl. Phys. **70**, 6149 (1991).
[17] W. Hume-Rothery and G. V. Raynor, *The Structure of Metals and Alloys*, 3rd ed. (The Institute of Metals, London, 1954).
[18] In the more modern American notation these would correspond to groups IV_A, V_A, and VI_A or to groups 14, 15, and 16.
[19] R. H. Herber, in *Chemical Mössbauer Spectroscopy*, edited by R. H. Herber (Plenum, New York, 1984), p. 204.